Removal of hexavalent chromium and methylene blue in aqueous solutions using activated carbon prepared from rubber seed shell

Kongsak Pattarith, Supattra Tangtubtim, Suphawarat Thupsuri*

Department of Chemistry, Faculty of Science, Buriram Rajabhat University, Buriram 31000, Thailand, emails: kongsak.pr@bru.ac.th https://orcid.org/0000-0001-5745-7325 (K. Pattarith), supattra.tt@bru.ac.th https://orcid.org/0009-0000-1539-3132 (S. Tangtubtim), suphawarat.pl@bru.ac.th https://orcid.org/0000-0001-8104-3755 (S. Thupsuri)

ABSTRACT

In the present study, the prepared rubber seed shell charcoal (RSS-CH) and activated carbon (RSS-AC) from rubber seed shell (RSS) were used as biosorbent for the removal of Cr(VI) and methylene blue (MB) from aqueous solutions. The surface characterizations of RSS, RSS-CH, and RSS-AC materials were performed using scanning electron microscopy, Fourier-transform infrared spectroscopy, and thermogravimetric analysis. The adsorption capacity of adsorbents was investigated by varying the pH, initial concentration, contact time, and temperature. The pH value on the solution had significant effect for the adsorption process, in which the optimum pH for adsorption of Cr(VI) and MB was 3 and 7, respectively. The adsorption isotherm of Cr(VI) was described by the Freundlich model while the adsorption process of MB fitted well with Langmuir model. The adsorption behavior of Cr(VI) and MB was described by pseudo-second-order kinetic model with $R^2 \sim 0.99$. Moreover, the maximum adsorption capacities of Cr(VI) on the RSS-CH and RSS-AC were 75.76 and 125 mg/g, respectively. For MB adsorption, maximum adsorption capacities on the RSS-CH and RSS-AC were 217.39 and 370.37 mg/g, respectively. The adsorption efficiency of Cr(VI) and MB on the RSS-AC showed greater than those of the RSS-CH. Thus, the RSS-AC is a suitable, alternative, and high adsorption efficiency adsorbent for the removal of heavy metal and dye contaminants in wastewater.

Keywords: Adsorption; Activated carbon; Charcoal; Rubber seed shell; Hexavalent chromium; Methylene blue

1. Introduction

Wastewater pollution from a variety of industries is discharged into the environment either organic (dyes, phenols, pesticides etc.) or inorganic pollutants (heavy metals, nitrates, phosphates etc.) [1–4]. It is an important problem to the environment pollution due to the effluent releasing of untreated wastewater from industries. Among the various environmental pollutants, heavy metals and dyes-containing wastewater cause damage to the human heath, fauna and flora, and aquatic ecosystem because of their non-biodegradability, strong oxidation capability, and high toxicity.

It can also transform as mutagenic and carcinogenic to living organisms when it long-term exposure [5]. Hexavalent chromium (Cr(VI)) is one of the most harmful effect among heavy metals, which is mainly produced from industrial processes such as electroplating, leather tanning, mining, textile, and ink [6–8]. Methylene blue (MB) is well-known for being an organic dye pollution which is widely used for extensive application in the colorize substance, especially in the textile industry [9–12]. Therefore, the removal of Cr(VI) and MB in the contaminated wastewater is essential to remove before their discharge into the aquatic environment.

Biological, chemical, and physical techniques that are used for the removal of heavy metals and dyes from

* Corresponding author.

industrial effluent including photocatalytic degradation [13], ion-exchange [14], membrane filtration [15], advance oxidation [16], and adsorption methods [17]. Among these methods, adsorption has been proved as one of the most efficient for water treatment process using different types of adsorbents such as polymer [4], resin [6], nano-composite [18], zeolite [19] as well as activated carbon [20]. Adsorption using activated carbon is extensively used as an adsorbent due to its high porosity, large specific surface area, and high adsorption capacity [21,22]. Activated carbon materials derived from agricultural waste have been investigated in several researches because of its low-cost, simple preparation, and simple regeneration [23,24]. The alternative low cost activated carbons from agricultural waste such as eucalyptus leaves [12], corn cob [17], edible fungus residue [25], tea [26], longan seed [27], *Peganum harmala* seeds [28], rice husk [29], acorn shell [30], groundnut shell [31], *Camellia oleifera* seed shell [32] etc. are used as adsorbent for the removal of Cr(VI) or MB in aqueous solution. However, the raw materials, activation agents, and preparation techniques have an effect on the activated carbon properties.

In general, the activated carbon is prepared by two different methods: physical activation and chemical activation. In the physical activation method, the activated charcoal or charcoal is produced by carbonized process at high temperature and is activated by steam or CO_2. In the chemical activation method, the raw material is impregnated with different activating agents including NaOH, KOH, H_3PO_4, H_2SO_4, $ZnCl_2$ etc. and then heated in inert atmosphere [12,33–35]. Both activation methods can modify the surface area, pore size, and chemical structure of materials [30,36].

In the present study, the adsorption potential of activated carbon from rubber seed shell (RSS) using $ZnCl_2$ was investigated. The rubber seed shell activated carbon (RSS-AC) was utilized for the removal of Cr(VI) and MB from aqueous solutions, and its adsorption performance was compared to that of rubber seed shell charcoal (RSS-CH). The various parameters of pH, initial concentration, contact time, and temperature were evaluated. Isotherm and kinetic adsorptions were determined to understand the adsorption process of Cr(VI) and MB onto the adsorbents. The regeneration efficiency of the adsorbents was also evaluated.

2. Materials and methods

2.1. Materials

The collected rubber seed shells were first washed with distilled water and then dried at 110°C overnight in an oven. The dried seeds were crushed to produce particles of the desired size of 2–4 mm. The crushed seeds were used as the precursor in the production of RSS-CH and RSS-AC. Zinc chloride, potassium dichromate, and methylene blue were obtained from Sigma-Aldrich Co., Ltd., Germany. All chemicals used are analytical grade.

2.2. Preparations of RSS-CH and RSS-AC

The RSS-CH was prepared through a carbonization process in an electric furnace at temperature of 600°C for 3 h. Afterward, the sample was washed with distilled water and then air dried at room temperature. For the preparation of RSS-AC, the RSS precursor was mixed with 20% w/v $ZnCl_2$ at an impregnation ratio of 1:2 (w/v), sonicated for 1 h, and refluxed for a further 6 h. The sample was washed with distilled water until it became neutral pH and then dried at 110°C overnight. The dried sample was activated in a furnace at 600°C for 3 h. Finally, the activated carbon was washed again with distilled water and then air dried at room temperature. The prepared RSS-AC was used for the adsorption studies of Cr(VI) and MB by comparison with charcoal adsorbent of RSS-CH.

2.3. Characterization of materials

The samples of the RSS, RSS-CH, and RSS-AC were determined the surface functional groups by Fourier-transform infrared (FTIR) spectrometer (Spectrum GX-1, Perkin Elmer Co., Ltd., UK). The surface distribution parameters of the adsorbents were performed by Brunauer–Emmett–Teller (BET) technique (TriStar II Plus 3.00, Micromeritics Co., Ltd., USA) at 77 K using N_2 gas adsorption. Scanning electron microscopy (TM40000Plus, Hitachi High-Tech Co., Ltd., Japan) was studied the surface morphology of the RSS, RSS-CH, and RSS-AC before adsorption. The thermal degradation characteristics of the adsorbents were evaluated by thermogravimetric (TG) analysis (SDT Q600, Lukens Drive, New Castle, DE 19720, USA) in N_2 atmosphere with a heating rate of 10°C/min from ambient temperature up to 900°C.

2.4. Adsorption experiments

The stock solutions of Cr(VI) and MB were prepared at concentration of 1,000 mg/L. The pH values of these stock solution were adjusted by adding with 0.1 M HCl or 0.1 M NaOH. The stock solutions were stored for further adsorption studies. Batch adsorption experiments were conducted for investigation the Cr(VI) and MB adsorption onto the RSS-CH and RSS-AC adsorbents. For each adsorption system, 50 mL of Cr(VI) or MB solutions was added with 0.01 g of adsorbent at various pH values under 150 rpm shaking and a controlled temperature of 30°C for 3 h. The parameters of adsorption process of Cr(VI) and MB, that is, initial concentration, temperature, and contact time were also investigated. The optimum conditions for the adsorptions of Cr(VI) and MB were used to determine the adsorption isotherm and kinetic studies. The concentrations of the residual heavy metal and dye after the adsorption progress were analyzed by PerkinElmer Lambda 12 UV-Visible Spectrometer at wavelength of 540 and 664 nm for Cr(VI) and MB adsorptions, respectively. The adsorption capacity at equilibrium for Cr(VI) and MB adsorptions, q_e (mg/g), can be expressed by Eq. (1):

$$q_e = \frac{(C_i - C_e)}{M} V \tag{1}$$

where C_i and C_e are the concentration of heavy metal or dye solutions at initial and given contact time (mg/L), respectively. V is the volume of heavy metal or dye solutions (L) and M is the amount of adsorbent (g). The adsorption capacity at a time t, q_t (mg/g), is defined by Eq. (2):

$$q_t = \frac{(C_i - C_t)}{M}V \tag{2}$$

where C_t is the concentration at contact time t (mg/L). Each batch experiment was conducted in triplicate.

3. Results and discussion

3.1. Characterization

The functional group analysis of the RSS, RSS-CH, and RSS-AC samples is shown in Fig. 1. The dominant peaks from FTIR of the RSS before and after the surface modification are also summarized in Table S1. It is shown that the broad peaks for RSS at 3,343 and 2,932 cm^{-1} are characteristic peaks of cellulose, lignin, and pectin corresponding to O-H and C-H stretching vibrations, respectively [37]. Compared with the spectrum of RSS, the peaks at 1,716–1,670 cm^{-1} are related with the C=O stretching vibration of carboxyl groups in hemicellulose of RSS, which disappear in RSS-CH and RSS-AC spectrum. The O-H peaks of RSS-CH and RSS-AC intensities decrease and observe at 3,396 and 3,398 cm^{-1}, respectively. The broad peaks at 1,588 and 1,564 cm^{-1} are also attributed C=O stretching vibration of alkene in RSS-CH and RSS-AC. Moreover, the C-O stretching peak of alcohol, carboxylic acid, or ether groups of RSS is clearly found at 1,034 cm^{-1} while the broad peaks are shifted to 1,170 and 1,160 cm^{-1} for RSS-CH and RSS-AC, respectively, this may be attributed to the change of FTIR spectrum of the RSS after surface modification.

The BET results of RSS-CH and RSS-AC were listed in Table 1. It is revealed that the surface area for RSS-AC is 972.16 m^2/g, which shows greater than that of RSS-CH
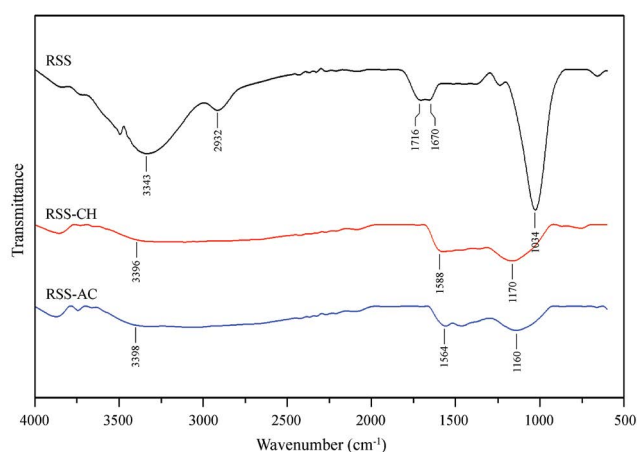
(628.45 m^2/g). The surface of RSS-AC is also high total pore volume, suggesting that the RSS was significantly damaged with ZnCl$_2$ agent during the activation procedure. The pores of RSS-CH and RSS-AC are 2.33 and 2.51 nm in diameter, respectively. The results imply that the material is predominantly mesoporous [38].

The surface morphologies of the RSS, RSS-CH, and RSS-AC are shown in Fig. 2. It can be seen that the RSS-CH and RSS-AC surfaces show numerous small pores, in comparison with the raw RSS material. Also, the surface of RSS under carbonization and chemical activation procedures shows small porous structure due to the cellulose, hemicellulose, and lignin components on the RSS surface are destroyed *via* heat and ZnCl$_2$.

Fig. 3. shows the TG and derivative (DTG) profiles for the RSS, RSS-CH, and RSS-AC samples. Owing to the evaporation of moisture, initial thermal degradation of all three samples appeared about 100°C. The major weight loss of the RSS sample (270°C–600°C) was decomposed on the main constituents of cellulose, hemicellulose, and lignin [21]. Moreover, TG curves for RSS-CH and RSS-AC exhibit more thermal stability than RSS, which may be the result of the dissociation of C-C bonds. The TG and DTG results also support that the surface of the RSS has been successfully modified.

3.2. Adsorption studies

3.2.1. Effect of pH

The effect of solution pH is an important parameter of bio-adsorption process and it controls the electrostatic interaction between the modified adsorbent surface and the heavy metal as well as dye molecule. Fig. 4a shows the pH of Cr(VI) adsorption under different pH condition (pH = 2–7) with a concentration of 250 mg/L. It can be observed that the acidic solution at pH ~ 3 is the optimum condition with adsorption capacity of 58.42 and 95.68 mg/g for Cr(VI) adsorption onto the RSS-CH and RSS-AC, respectively. Normally, the dominant forms of $HCrO_4^-$ and $Cr_2O_7^{2-}$ are found in the solution at pH 2–6 [39]. Therefore, the adsorbent surfaces are protonated by H$^+$ ions, which favor the electrostatic attraction between anionic forms and the positively charged surfaces. When increase pH values, the protonation of the surface is weakened with the predominance of OH$^-$ ions, leading to an increase in electrostatic repulsion between negatively charged ions and adsorbent surfaces [40]. As a result, the adsorption capacities of Cr(VI) decreased with increasing of pH solution, then showed a rapidly decrease after pH 4.

Fig. 4b shows the effect of pH values in the range of 3 to 9 with concentration of 750 mg/L. At a low pH, the existence of H$^+$ ions in the solution causes a positive charge on the adsorbent surface, which leads to the competition with

Fig. 1. Fourier-transform infrared spectra of RSS, RSS-CH, and RSS-AC.

Table 1
Surface distribution parameters of RSS-CH and RSS-AC

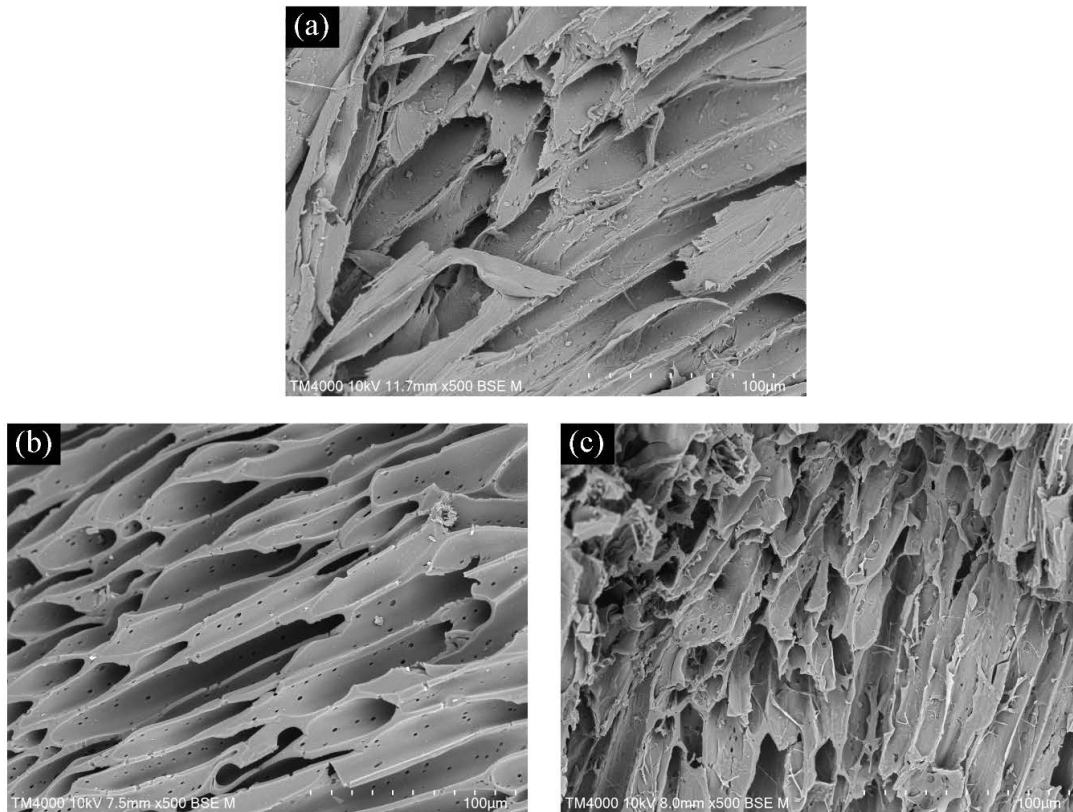| Adsorbents	Brunauer–Emmett–Teller surface area (m^3/g)	Total pore volume (cm^3/g)	Average pore diameter (nm)
RSS-CH	628.45	0.46	2.33
RSS-AC	972.16	0.72	2.51

Fig. 2. Scanning electron microscopy images of (a) RSS, (b) RSS-CH, and (c) RSS-AC.
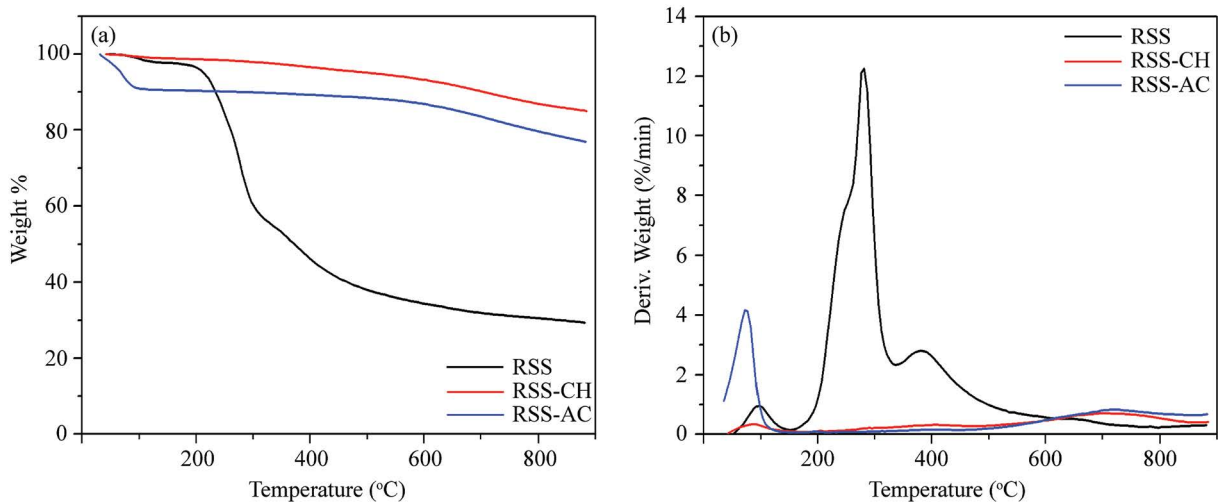

Fig. 3. (a) Dynamic thermogravimetric and (b) derivative curves of RSS, RSS-CH, and RSS-AC under a heating rate of 10°C/min in N_2 atmosphere.

cationic dye molecules. The attractive force between the adsorbent and MB is weakened, resulting in a lower adsorption capacity of dye. However, the positively charge surface decreases at a higher pH, which facilitates to the adsorption of cationic dye. The optimum value of pH is 7 with adsorption capacity of 205.05 and 316.16 mg/g for MB adsorption onto the RSS-CH and RSS-AC, respectively.

3.2.2. Effect of initial concentration

The variation of the initial concentration of Cr(VI) and MB on the adsorption capacity is shown in Fig. 5. It is observed that the adsorption capacities of Cr(VI) and MB rapidly increase at the initial stage because the ratio of Cr(VI) or MB molecules to the unoccupied active site of
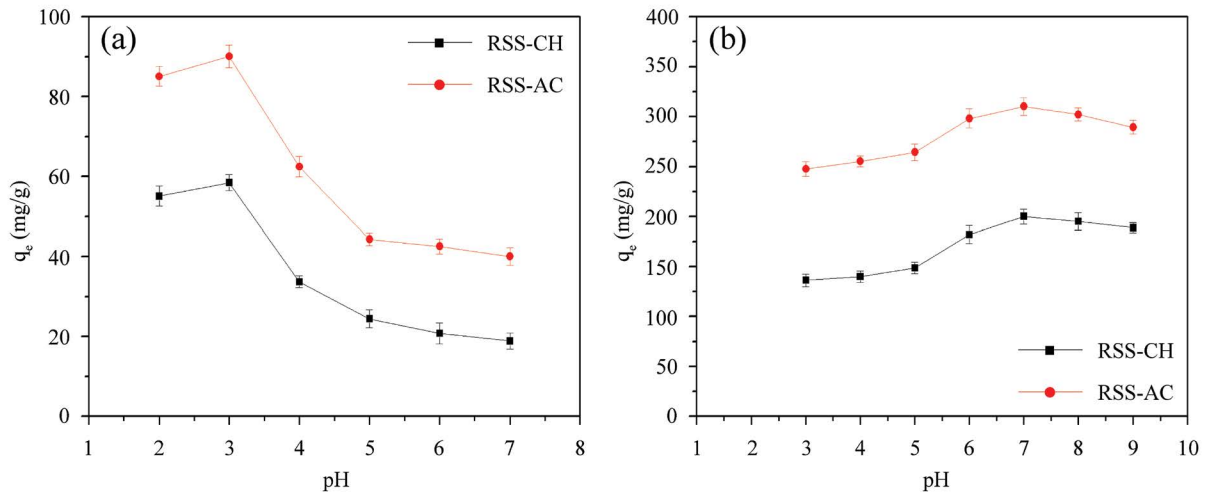
Fig. 4. Effect of pH values for (a) Cr(VI) and (b) MB adsorptions on the RSS-CH and RSS-AC.
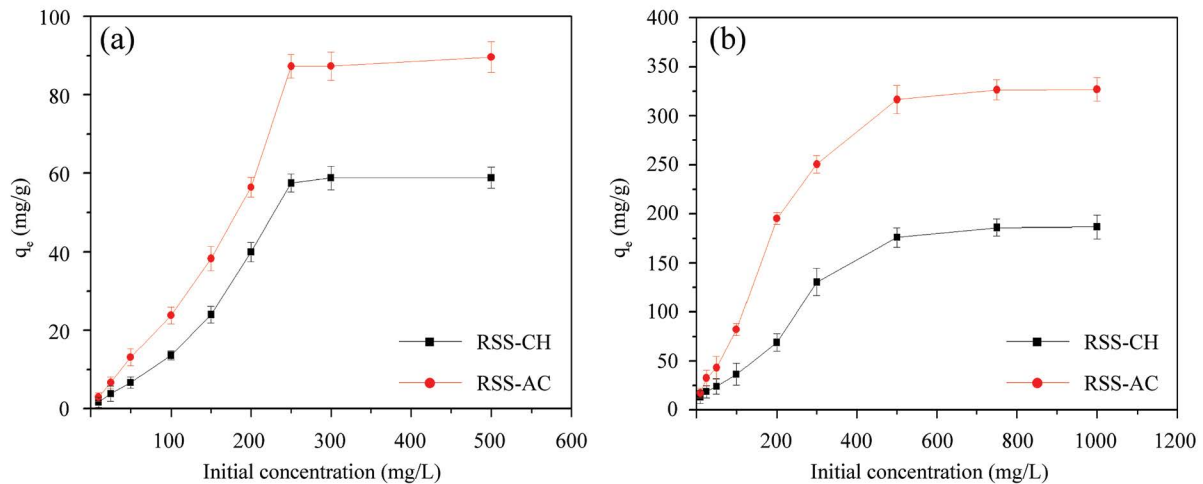

Fig. 5. Effect of initial concentrations for (a) Cr(VI) and (b) MB adsorptions on the RSS-CH and RSS-AC.

the adsorbent is low. At higher concentrations, more adsorbate molecules are transported to the surface saturation of the binding sites [25]. Therefore, the adsorption efficiencies increase and reach equilibrium at 250 and 750 mg/L for Cr(VI) and MB adsorptions, respectively.

3.2.3. Effect of contact time and temperature

The amounts of Cr(VI) and MB adsorbed onto the adsorbent surfaces with different contact times at temperatures of 30°C, 40°C, and 50°C are shown in Fig. 6. The capacity of Cr(VI) and MB adsorbed onto the adsorbents rapidly increases with the contact time increasing from 10 to 50 min. Then, the amount of heavy metal and dye molecules on the surface gradually decreases and reaches the equilibrium state at a contact time ≥75 min. Initially, the available adsorption sites and the adsorption capacities reduce in the later stage, leading to the saturation sites on the surface and the slow diffusion of adsorbate particles into the porous structure [26]. The effect of temperature at equilibrium indicates

that the adsorption capacity of heavy metal and dye on both adsorbents at 50°C is greater than those at other temperatures. Thus, the adsorption process is endothermic. In addition, the absorption efficiency of RSS-AC is clearly higher than those for RSS-CH, suggesting that adsorption sites and surface areas of RSS increase after chemical modification.

3.3. Adsorption isotherms

The mechanisms of the adsorption at equilibrium are described with adsorption isotherm models. The Langmuir and Freundlich adsorption isotherms are extensively utilized to evaluate the interaction behavior during the adsorption process via the curve fitting method [41]. The Langmuir isotherm model assumes monolayer coverage of heavy metal and dye molecules onto the homogeneous surface. The linear form of the Langmuir equation is expressed by Eq. (3):

$$\frac{C_e}{q_e} = \frac{C_e}{Q_m} + \frac{1}{bQ_m} \tag{3}$$

where C_e is the concentration equilibrium of heavy metal and dye (mg/L), q_e is the equilibrium adsorption capacity (mg/g), Q_m is the maximum adsorption capacity (mg/g), and b is the Langmuir binding constant (L/mg). A further analysis of the Langmuir hypothesis can be estimated using a dimensionless constant, (R_L), and it is expressed by Eq. (4):

$$R_L = \frac{1}{1 + bC_0} \tag{4}$$

where C_0 is the initial concentration of heavy metal and dye (mg/L). The R_L value describes the suitable for the adsorption isotherm in the present study, in which it is unfavorable ($R_L > 1$), favorable ($0 < R_L < 1$), linear ($R_L = 1$), and irreversible adsorptions ($R_L = 0$). The calculated values of 0–1 represent favorable for adsorption behavior (Table 2).

The Freundlich isotherm model is suitable for the heterogeneous adsorption on the surface. The linear Freundlich equation is expressed by Eq. (5) [42]:

$$\ln q_e = \ln K_F + \frac{1}{n} \ln C_e \tag{5}$$

where K_F and n are the Freundlich constant and Freundlich exponent, respectively, in which n value relate to the adsorption capacity and adsorption strength. The obtained values of $1/n < 1$ indicate favorable adsorption process.

The parameters of Langmuir and Freundlich adsorption isotherms of the Cr(VI) and MB adsorptions can be obtained from the slope and intercept of the linear plot and are summarized in Table 2 and shown in Figs. S1 and S2. As considered from R^2, the adsorption behavior of Cr(VI) on the surface provided fits well with Freundlich isotherm ($R^2 > 0.99$), indicating that the adsorption of Cr(VI) is multilayer adsorption onto the heterogeneous surface. Meanwhile, the adsorption isotherm of MB on the surface fits better to Langmuir isotherm, suggesting that the adsorption of MB onto the surfaces are distributed with monolayer coverage. Moreover, the Cr(VI) and MB adsorption efficiencies on the RSS-AC surface are higher than that of the RSS-CH surface. It can be also concluded that the RSS-AC has a high affinity for the active sites on the surface of adsorbent.

The maximum adsorption capacity of Cr(VI) and MB adsorbed on RSS-CH and RSS-AC are compared with other adsorbents, as shown in Table 3 [17,20,26,27,31,32,34,35,40,43–49]. It is revealed that the maximum adsorption capacity of
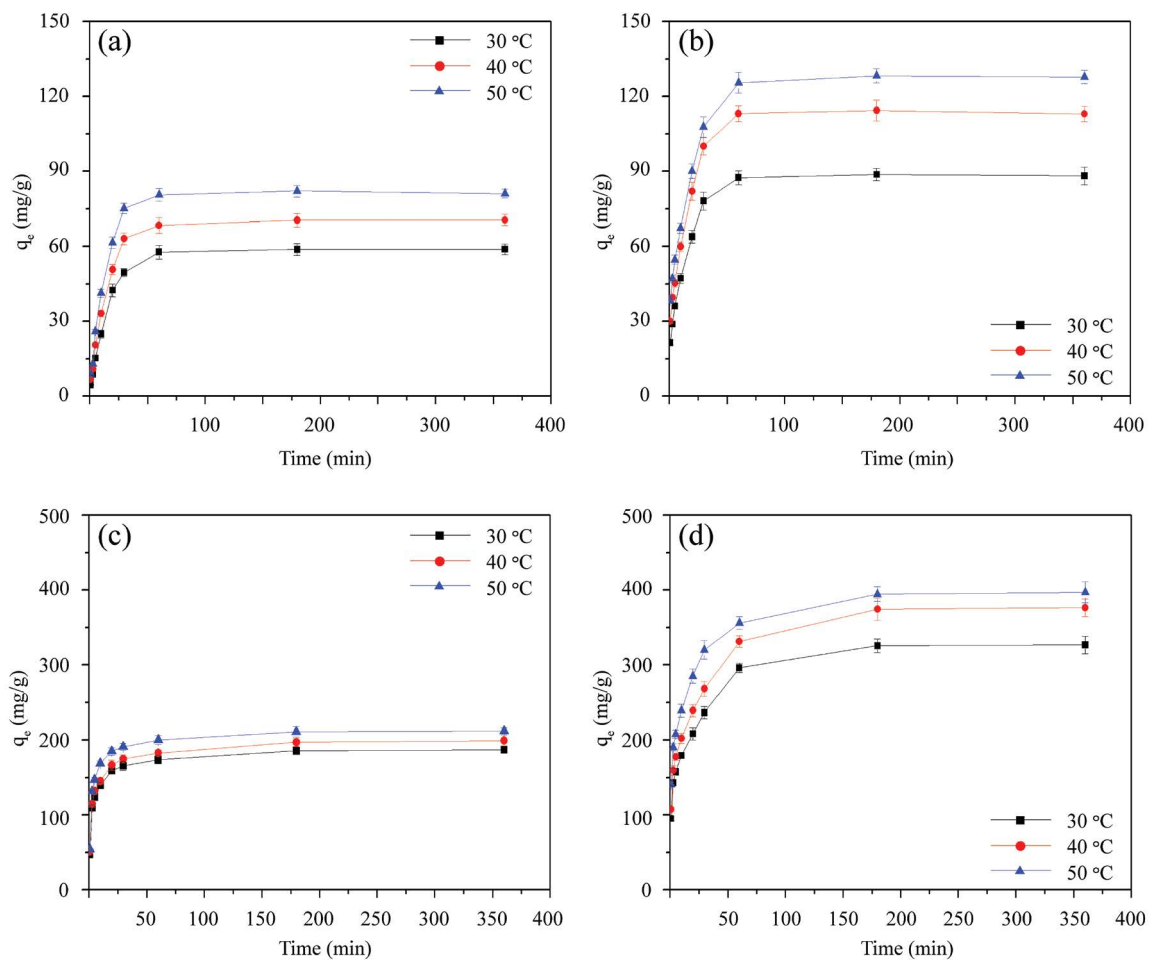

Fig. 6. Effect of contact time at different temperatures for Cr(VI) adsorption on the (a) RSS-CH and (b) RSS-AC. Effect of contact time at different temperatures for MB adsorption on the (c) RSS-CH and (d) RSS-AC.

Table 2
Langmuir and Freundlich isotherm parameters for the Cr(VI) and MB adsorptions on the RSS-CH and RSS-AC

Adsorbent	Langmuir equation				Freundlich equation			
	R_L	Q_m (mg/g)	b (L/mg)	R^2	K_F (L/g)	n (L/mg)	$1/n$ (mg/L)	R^2
Cr(VI) adsorption								
RSS-CH	0.14	75.76	7.92×10^{-3}	0.8729	0.19	1.09	0.92	0.9990
RSS-AC	0.18	125.00	5.92×10^{-3}	0.7937	0.37	1.10	0.90	0.9971
MB adsorption								
RSS-CH	0.33	217.39	7.99×10^{-3}	0.9940	5.92	2.67	0.37	0.8986
RSS-AC	0.32	370.37	8.39×10^{-3}	0.9967	6.31	1.84	0.54	0.9017

RSS-AC displays higher than those of various adsorbents for Cr(VI) and MB adsorptions. In addition, there is no investigation of the rubber seed shell as an adsorbent for the Cr(VI) and MB removals. Therefore, activated carbon prepared from rubber seed shell in this work can be considered promising adsorbent for removal of heavy metal and dye contaminants in aqueous solution.

3.4. adsorption kinetics

To study the kinetic mechanisms of the equilibrium data in term of the order of the rate constant, the pseudo-first-order and pseudo-second-order kinetics are applied [50].

The linear form of the pseudo-first-order kinetic is calculated:

$$\ln\left(q_e - q_t\right) = \ln q_e - k_1 t \qquad (6)$$

where q_e and q_t are the amounts of heavy metal and dye adsorbed on the surface at equilibrium and at time t (mg/g), respectively. k_1 is pseudo-first-order adsorption constant (min⁻¹). The value kinetic parameters of k_1 and q_e can be obtained from the plot of $\ln(q_e - q_t)$ vs. t with different temperatures (Fig. S3).

The linear form of the pseudo-second-order kinetic can be presented:

$$\frac{t}{q_t} = \frac{1}{k_2 q_e^2} + \frac{t}{q_e} \qquad (7)$$

where k_2 is the pseudo-second-order adsorption constant (g/mg·min). The kinetic parameters of k_2 and q_e can be obtained from the plot of $1/q_t$ vs. t (Fig. S4). The values of the kinetic parameters under different temperature were calculated from slope and intercept of the linear plots and are summarized in Table 4. It is revealed that the kinetic adsorptions of Cr(VI) and MB on both the RSS-CH and RSS-AC fit better with pseudo-second-order model. This indicates that the adsorption rate was dependent on both adsorbate molecules and adsorbent surfaces. Also, the calculated of q_e(cal.) is match well with the experimental results.

3.5. Adsorption mechanism

Based on the characterization and adsorption results of Cr(VI) and MB adsorptions onto the adsorbents, the pore

Table 3
Comparison of the maximum adsorption capacities of Cr(VI) and MB adsorptions with different adsorbents

Adsorbents	q_{max} (mg/g)	References
Cr(VI) adsorption		
Mango kernel activated carbon	7.80	[43]
Almond green hull	10.12	[44]
Modified pomelo peel	21.55	[45]
Longan seed activated carbon	35.02	[27]
Apple peel activated carbon	36.01	[40]
Aerobically digested activated sludge	70.15	[46]
Modified groundnut hull	131.00	[31]
Camellia oleifera seed shell	307.26	[32]
Rubber seed shell charcoal	75.76	This study
Rubber seed shell activated carbon	125.00	This study
MB adsorption		
Fox nutshell activated carbon	75.37	[47]
Tea waste activated carbon	147.06	[26]
Karanj fruit hull activated carbon	239.40	[48]
Magnetized palm shell-waste activated carbon	163.30	[49]
Corn cob activated carbon	333.00	[17]
Ulva lactuca activated carbon	344.83	[20]
Rattan waste activated carbon	359.00	[35]
Hazelnut husk activated carbon	476.20	[34]
Rubber seed shell charcoal	217.39	This study
Rubber seed shell activated carbon	370.37	This study

structures of RSS-CH and RSS-AC provided numerous adsorption sites, which led to the Cr(VI) and MB adsorptions onto the surface. For the Cr(VI) adsorption at low pH optimum, the $HCrO_4^-$ form in dilute Cr(VI) solution was adsorbed with more positively charged active sites on the RSS-CH and RSS-AC by electrostatic attraction, which was supported by previously reported studies [6,7,32,40,44]. For the MB adsorption, the functional groups of O-H and C=C on the adsorbent surfaces and MB structures were interacted during adsorption through H-bonding and electrostatic

Table 4
Pseudo-first-order and pseudo-second-order kinetic parameters for the Cr(VI) and MB adsorptions on the RSS-CH and RSS-AC

| Adsorbent	T (°C)	q_e(exp) (mg/g)	Pseudo-first-order			Pseudo-second-order		
			q_e(cal) (mg/g)	k_1 (min^{-1})	R^2	q_e(cal) (mg/g)	k_2 (g/mg·min)	R^2
Cr(VI) adsorption								
RSS-CH	30	57.77	60.69	6.43×10^{-2}	0.9132	54.95	1.25×10^{-3}	0.9943
	40	68.40	78.70	6.98×10^{-2}	0.9195	69.93	1.10×10^{-3}	0.9949
	50	80.56	82.16	7.76×10^{-2}	0.9211	80.65	1.09×10^{-3}	0.9975
RSS-AC	30	87.45	77.56	7.19×10^{-2}	0.9671	88.49	1.05×10^{-3}	0.9901
	40	113.05	95.85	5.84×10^{-2}	0.9734	113.64	7.97×10^{-4}	0.9950
	50	125.49	102.51	5.00×10^{-2}	0.9519	120.48	8.89×10^{-4}	0.9934
MB adsorption								
RSS-CH	30	173.69	100.64	6.77×10^{-2}	0.8609	166.67	2.17×10^{-4}	0.9935
	40	182.96	110.51	5.72×10^{-2}	0.8835	181.82	2.19×10^{-4}	0.9928
	50	200.08	138.55	6.29×10^{-2}	0.8594	208.33	1.88×10^{-4}	0.9974
RSS-AC	30	296.08	168.49	9.01×10^{-2}	0.8509	270.27	9.48×10^{-5}	0.9930
	40	331.09	207.29	1.01×10^{-1}	0.8337	333.33	6.45×10^{-5}	0.9845
	50	355.96	259.41	9.77×10^{-2}	0.8864	357.14	6.00×10^{-5}	0.9705
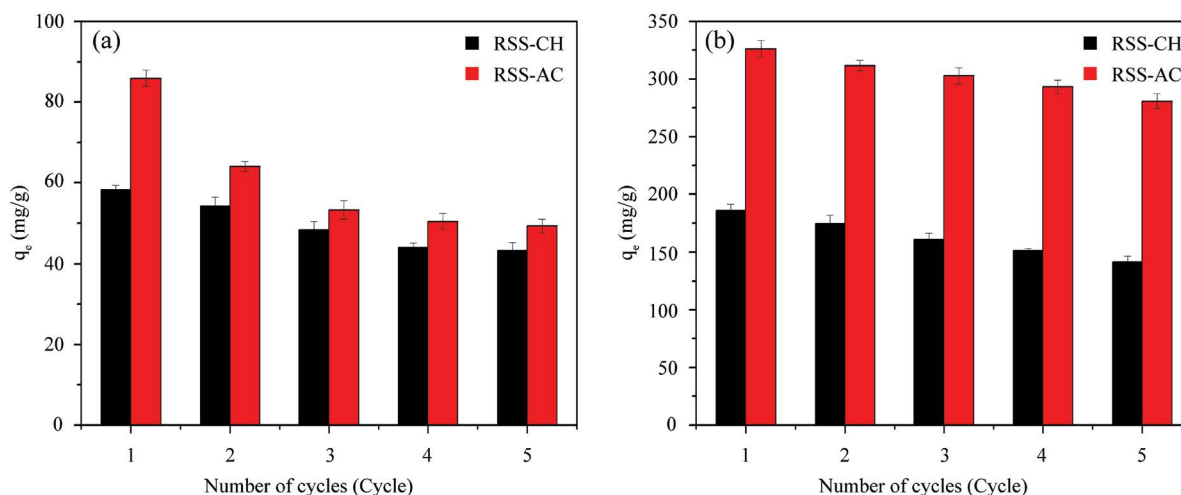
Fig. 7. Regeneration plots of (a) Cr(VI) and (b) MB adsorptions.

interaction. Also, π–π bond occur between aromatic rings of the MB structure and aromatic rings of the adsorbent [12,25,33,47]. As a results, this greatly increases of the MB adsorption onto the surfaces.

3.6. Regeneration studies

The regenerative ability of an adsorbent in the desorption solution of 0.1 M HCl is an important for reducing the cost of the system. The addition of acid may be caused more active sites portion of the adsorbents. Fig. 7 shows that the reusability performance of the surfaces was determined by repeating the adsorption of five cycles using 250 mg/L for the initial Cr(VI) concentration and 750 mg/L for the initial MB concentration. After five regenerations, the Cr(VI) adsorption capacities on the RSS-CH and RSS-AC decrease from

58.26 to 43.36 mg/g and 85.96 to 49.29 mg/g, respectively. Whereas, MB adsorption capacities on the RSS-CH and RSS-AC decrease from 186.10 to 141.75 mg/g and 326.36 to 281.04 mg/g, respectively. These result shown that RSS-CH and RSS-AC had a good reusability performance after reuse. Thus, the effective bioadsorbent of RSS-CH and RSS-AC could be utilized as a recyclable adsorbent for the Cr(VI) and MB removals.

Moreover, the Cr(VI) and MB-containing on the adsorbent should be appropriately eliminated after the adsorption process. Ghosh et al. [33] studied the disposal of MB molecules from adsorbent by incineration technique, which can produce the ash from the combustion of adsorbent wastes at high temperatures. The ash obtained may be used as an ingredient in brick manufacturing [7]. Meanwhile, metal molecules cannot be completely destroyed with this method.

Therefore, the metal contamination in the ash from incineration was performed using pyrometallurgical process with three steps, that is, leaching with acid solution, purification, and metal recovery, respectively [51].

4. Conclusion

In this study, rubber seed shell charcoal and rubber seed shell activated carbon were used for the removal of Cr(VI) and MB from aqueous solution. The results indicated that the RSS-AC has a higher adsorption efficiency with a BET surface area of 972.16 m²/g. The adsorption process of Cr(VI) showed a good fit in the Freundlich isotherm while adsorption of MB fitted well with Langmuir isotherm. The effect of pH on solution reveals that the acidic solution at pH ~ 3 was the optimum condition for Cr(VI) adsorption while neutral pH was suitable for MB adsorption. The adsorption behavior of Cr(VI) and MB was explained by pseudo-second-order kinetic with R^2 ~ 0.99. The maximum adsorption capacities of Cr(VI) on the RSS-CH and RSS-AC were 75.76 and 125.00 mg/g, respectively. For MB adsorption, maximum adsorption capacities on the RSS-CH and RSS-AC were 217.39 and 370.37 mg/g, respectively. Therefore, the RSS-AC exhibited high adsorption efficiency when compared with RSS-CH. Based on these results, the RSS-AC is the effective adsorbent for use in the removal of heavy metal and dye contaminants in wastewater.

Acknowledgement

References

[1] G. Indrajit, S. Kar, T. Chatterjee, N. Bar, S.K. Das, Adsorptive removal of Safranin-O dye from aqueous medium using coconut coir and its acid-treated forms: adsorption study, scale-up design, MPR and GA-ANN modeling, Sustainable Chem. Pharm., 19 (2021) 100374, doi: 10.1016/j.scp.2021.100374.

[2] X. Yin, Y. Jiang, Y. Tan, X. Meng, H. Sun, N. Wang, Co-transport of graphene oxide and heavy metal ions in surface-modified porous media, Chemosphere, 218 (2019) 1–13.

[3] Y. Liu, X. Zhang, J. Wang, A critical review of various adsorbents for selective removal of nitrate from water: structure, performance and mechanism, Chemosphere, 291 (2022) 132728, doi: 10.1016/j.chemosphere.2021.132728.

[4] Z. Abdeen, S.G. Mohammad, Study of the adsorption efficiency of an eco-friendly carbohydrate polymer for contaminated aqueous solution by organophosphorus pesticide, Open J. Org. Polym. Mater., 4 (2014) 16–28.

[5] E. Altintig, S. Cabukcu, Performance of zinc hydroxide coated activated carbon in the removal of methylene blue from aqueous solutions, Desal. Water Treat., 269 (2022) 188–199.

[6] F.-B. Liang, Y.-L. Song, C.-P. Huang, J. Zhang, B.-H. Chen, Adsorption of hexavalent chromium on a lignin-based resin: equilibrium, thermodynamics, and kinetics, J. Environ. Chem. Eng., 1 (2013) 1301–1308.

[7] S. Sarkar, N. Bar, S.K. Das, Cr(VI) and Cu(II) removal from aqueous solution in fixed bed column using rice bran; experimental, statistical and GA modelling, J. Indian Chem. Soc., 98 (2021) 100216, doi: 10.1016/j.jics.2021.100216.

[8] R. Saha, R. Nandi, B. Saha, Sources and toxicity of hexavalent chromium, J. Coord. Chem., 64 (2011) 1782–1806.

[9] G. Manikandan, P. Senthil Kumar, A. Saravanan, Modelling and analysis on the removal of methylene blue dye from aqueous solution using physically/chemically modified *Ceiba pentandra* seeds, J. Ind. Eng. Chem., 62 (2018) 446–461.

[10] R.P. Pawar, Lalhmunsiama, P. Gupta, S.Y. Sawant, B. Shahmoradi, S.-M. Lee, Porous synthetic hectorite clay-alginate composite beads for effective adsorption of methylene blue dye from aqueous solution, Int. J. Biol. Macromol., 114 (2018) 1315–1324.

[11] S.E. Moradi, Microwave assisted preparation of sodium dodecyl sulphate (SDS) modified ordered nanoporous carbon and its adsorption for MB dye, J. Ind. Eng. Chem., 20 (2014) 208–215.

[12] K. Ghosh, N. Bar, A.B. Biswas, S.K. Das, Removal of methylene blue by H_3PO_4 treated eucalyptus leaves: study of fixed bed column and GA-ANN modeling, Sustainable Chem. Pharm., 29 (2022) 100774, doi: 10.1016/j.scp.2022.100774.

[13] M. Rashidi, S. Maryam Sajjadi, H.Z. Mousavi, Kinetic analysis of azo dye decolorization during their acid–base equilibria: photocatalytic degradation of tartrazine and sunset yellow, React. Kinet. Mech. Catal., 128 (2019) 555–570.

[14] H. Masood, S. Zafar, H. ur Rehman, M.I. Khan, H.B. Ahmad, A. Naz, W. Hassan, M.H. Lashari, Adsorptive removal of anionic dyes in aqueous binary mixture by anion exchange membrane, Desal. Water Treat., 194 (2020) 248–258.

[15] H. Xiang, X. Min, C.-J. Tang, M. Sillanpää, F. Zhao, Recent advances in membrane filtration for heavy metal removal from wastewater: a mini review, J. Water Process Eng., 49 (2022) 103023, doi: 10.1016/j.jwpe.2022.103023.

[16] J. Liang, L. Zhang, M. Ye, Z. Guan, J. Huang, J. Liu, L. Li, S. Huang, S. Sun, Evaluation of the dewaterability, heavy metal toxicity and phytotoxicity of sewage sludge in different advanced oxidation processes, J. Cleaner Prod., 265 (2020) 121839, doi: 10.1016/j.jclepro.2020.121839.

[17] A. Medhat, H.H. El-Maghrabi, A. Abdelghany, N.M. Abdel Menem, P. Raynaud, Y.M. Moustafa, M.A. Elsayed, A.A. Nada, Efficiently activated carbons from corn cob for methylene blue adsorption, Appl. Surf. Sci. Adv., 3 (2021) 100037, doi: 10.1016/j.apsadv.2020.100037.

[18] M. Tuzen, A. Sarı, T.A. Saleh, Response surface optimization, kinetic and thermodynamic studies for effective removal of Rhodamine B by magnetic AC/CeO₂ nanocomposite, J. Environ. Manage., 206 (2018) 170–177.

[19] S. Radoor, J. Karayil, A. Jayakumar, J. Parameswaranpillai, S. Siengchin, Removal of methylene blue dye from aqueous solution using PDADMAC modified ZSM-5 zeolite as a novel adsorbent, J. Polym. Environ., 29 (2021) 3185–3198.

[20] A. El Nemr, A.G.M. Shoaib, A. El Sikaily, A.E.-D.A. Mohamed, A.F. Hassan, Evaluation of cationic methylene blue dye removal by high surface area mesoporous activated carbon derived from *Ulva lactuca*, Environ. Processes, 8 (2021) 311–332.

[21] S. Mandal, J. Calderon, S.B. Marpu, M.A. Omary, S.Q. Shi, Mesoporous activated carbon as a green adsorbent for the removal of heavy metals and Congo red: characterization, adsorption kinetics, and isotherm studies, J. Contam. Hydrol., 243 (2021) 103869, doi: 10.1016/j.jconhyd.2021.103869.

[22] A. Saha, B.B. Basak, M. Ponnuchamy, Performance of activated carbon derived from *Cymbopogon winterianus* distillation waste for scavenging of aqueous toxic anionic dye Congo red: comparison with commercial activated carbon, Sep. Sci. Technol., 55 (2020) 1970–1983.

[23] S. Mashhadi, H. Javadian, M. Ghasemi, T.A. Saleh, V.K. Gupta, Microwave-induced H_2SO_4 activation of activated carbon derived from rice agricultural wastes for sorption of methylene blue from aqueous solution, Desal. Water Treat., 57 (2016) 21091–21104.

[24] R. Thotagamuge, M.R.R. Kooh, A.H. Mahadi, C.M. Lim, M. Abu, A. Jan, A.H. Abu Hanipah, Y.Y. Khiong, A. Shofry, Copper modified activated bamboo charcoal to enhance adsorption of heavy metals from industrial wastewater, Environ. Nanotechnol. Monit. Manage., 16 (2021) 100562, doi: 10.1016/j.enmm.2021.100562.

[25] H. Li, L. Liu, J. Cui, J. Cui, F. Wang, F. Zhang, High-efficiency adsorption and regeneration of methylene blue and aniline

onto activated carbon from waste edible fungus residue and its possible mechanism, RSC Adv., 10 (2020) 14262–14273.

[26] F.J. Tuli, A. Hossain, A.K.M. Fazle Kibria, A.R.M. Tareq, S.M.M.A. Mamun, A.K.M. Atique Ullah, Removal of methylene blue from water by low-cost activated carbon prepared from tea waste: a study of adsorption isotherm and kinetics, Environ. Nanotechnol. Monit. Manage., 14 (2020) 100354, doi: 10.1016/j.enmm.2020.100354.

[27] J. Yang, M. Yu, W. Chen, Adsorption of hexavalent chromium from aqueous solution by activated carbon prepared from longan seed: kinetics, equilibrium and thermodynamics, J. Ind. Eng. Chem., 21 (2015) 414–422.

[28] N. Nasseha, R. Khosravi, G.A. Rumman, M. Ghadirian, H. Eslami, M. Khoshnamvand, T.J. Al-Musawi, A. Khosravi, Adsorption of Cr(VI) ions onto powdered activated carbon synthesized from *Peganum harmala* seeds by ultrasonic waves activation, Environ. Technol. Innovation, 21 (2021) 101277, doi: 10.1016/j.eti.2020.101277.

[29] T. Mitra, N. Bar, S.K. Das, Rice husk: green adsorbent for Pb(II) and Cr(VI) removal from aqueous solution—column study and GA–NN modeling, SN Appl. Sci., 1 (2019) 486.

[30] E. Altıntıg, H. Altundag, M. Tuzen, A. Sarı, Effective removal of methylene blue from aqueous solutions using magnetic loaded activated carbon as novel adsorbent, Chem. Eng. Res. Des., 122 (2017) 151–163.

[31] S.O. Owalude, A.C. Tella, Removal of hexavalent chromium from aqueous solutions by adsorption on modified groundnut hull, Beni-Suef Univ. J. Basic Appl. Sci., 5 (2016) 377–388.

[32] H. Guo, C. Bi, C. Zeng, W. Ma, L. Yan, K. Li, K. Wei, *Camellia oleifera* seed shell carbon as an efficient renewable bio-adsorbent for the adsorption removal of hexavalent chromium and methylene blue from aqueous solution, J. Mol. Liq., 249 (2018) 629–636.

[33] K. Ghosh, N. Bar, A.B. Biswas, S.K. Das, Removal of methylene blue (AQ) using untreated and acid-treated eucalyptus leaves and GA-ANN modelling, Can. J. Chem. Eng., 97 (2019) 2883–2898.

[34] G. Karaçetin, S. Sivrikaya, M. Imamoglu, Adsorption of methylene blue from aqueous solutions by activated carbon prepared from hazelnut husk using zinc chloride, J. Anal. Appl. Pyrolysis, 110 (2014) 270–276.

[35] M.A. Islam, M.J. Ahmed, W.A. Khanday, M. Asif, B.H. Hameed, Mesoporous activated carbon prepared from NaOH activation of rattan (*Lacosperma secundiflorum*) hydrochar for methylene blue removal, Ecotoxicol. Environ. Saf., 138 (2017) 279–285.

[36] F. Ali, N. Ali, I. Bibi, A. Said, S. Nawaz, Z. Ali, S.M. Salman, H.M.N. Iqbal, M. Bilal, Adsorption isotherm, kinetics and thermodynamic of acid blue and basic blue dyes onto activated charcoal, Case Stud. Chem. Environ. Eng., 2 (2020) 100040, doi: 10.1016/j.cscee.2020.100040.

[37] J. Zhuang, M. Li, Y. Pu, A.J. Ragauskas, C.G. Yoo, Observation of potential contaminants in processed biomass using Fourier transform infrared spectroscopy, Appl. Sci., 10 (2020) 4345, doi: 10.3390/app10124345.

[38] C. Anyika, N.A.M. Asri, Z.A. Majid, A. Yahya, J. Jaafar, Synthesis and characterization of magnetic activated carbon developed from palm kernel shells, Nanotechnol. Environ. Eng., 2 (2017) 16.

[39] S. Tangtubtim, S. Saikrasun, Adsorption behavior of polyethyleneimine-carbamate linked pineapple leaf fiber for Cr(VI) removal, Appl. Surf. Sci., 467–468 (2019) 596–607.

[40] I. Enniya, L. Rghioui, A. Jourani, Adsorption of hexavalent chromium in aqueous solution on activated carbon prepared from apple peels, Sustainable Chem. Pharm., 7 (2018) 9–16.

[41] I. Langmuir, The adsorption of gases on plane surfaces of glass, mica and platinum, J. Am. Chem. Soc., 40 (1918) 1361–1403.

[42] H. Freundlich, Uber die adsorption in Losungen, Zeitschrift für Physikalische Chemie, Z. Phys. Chem., 57 (1906) 385–470.

[43] M.K. Rai, G. Shahi, V. Meena, R. Meena, S. Chakraborty, R.S. Singh, B.N. Rai, Removal of hexavalent chromium Cr(VI) using activated carbon prepared from mango kernel activated with H_3PO_4, Resour.-Effic. Technol., 2 (2016) S63–S70.

[44] N. Nasseh, L. Taghavi, B. Barikbin, A.R. Harifi-Mood, The removal of Cr(VI) from aqueous solution by almond green hull waste material: kinetic and equilibrium studies, J. Water Reuse Desal., 7 (2017) 449–460.

[45] Q. Wang, C. Zhou, Y.J. Kuang, Z.H. Jiang, M. Yang, Removal of hexavalent chromium in aquatic solutions by pomelo peel, Water Sci. Eng., 13 (2020) 65–73.

[46] F. Gorzin, A.A. Ghoreyshi, Synthesis of a new low-cost activated carbon from activated sludge for the removal of Cr(VI) from aqueous solution: equilibrium, kinetics, thermodynamics and desorption studies, Korean J. Chem. Eng., 30 (2013) 1594–1602.

[47] A. Kumar, H.M. Jena, Removal of methylene blue and phenol onto prepared activated carbon from Fox nutshell by chemical activation in batch and fixed-bed column, J. Cleaner Prod., 137 (2016) 1246–1259.

[48] M.A. Islam, S. Sabar, A. Benhouria, W.A. Khanday, M. Asif, B.H. Hameed, Nanoporous activated carbon prepared from karanj (*Pongamia pinnata*) fruit hulls for methylene blue adsorption, J. Taiwan Inst. Chem. Eng., 74 (2017) 96–104.

[49] K.T. Wong, N.C. Eu, S. Ibrahim, H. Kim, Y. Yoon, M. Jang, Recyclable magnetite-loaded palm shell-waste based activated carbon for the effective removal of methylene blue from aqueous solution, J. Cleaner Prod., 115 (2016) 337–342.

[50] Y.S. Ho, G. McKay, Sorption of dye from aqueous solution by peat, Chem. Eng. Sci., 70 (1998) 115–124.

[51] U.U. Jadhav, H. Hocheng, A review of recovery of metals from industrial waste, J. Achiev. Mater. Manuf. Eng., 54 (2012) 159–167.

Supplementary information

Table S1
Dominant peaks from Fourier-transform infrared spectroscopy of the RSS, RSS-CH, and RSS-AC

Functional groups	Characteristic absorption (cm^{-1})		
	RSS	RSS-CH	RSS-AC
O-H stretching of alcohol group	3,343	3,396	3,398
C-H stretching	2,932	–	–
C=O stretching of carboxyl group	1,716–1,670	–	–
C=C stretching of alkene	–	1,588	1,564
C-O stretching of alcohol, carboxylic acid, or ether groups	1,034	1,160	1,170
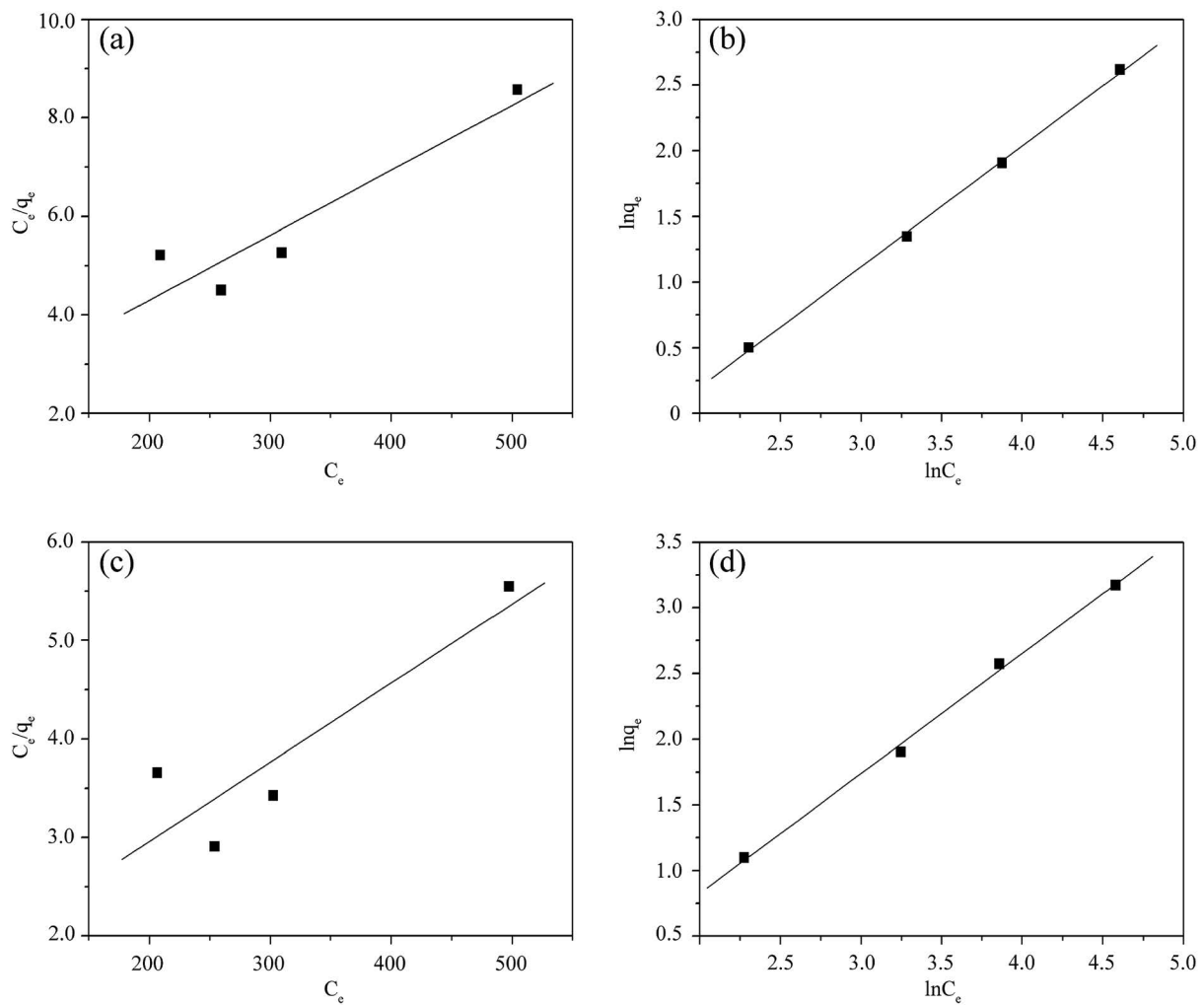
Fig. S1. (a) Langmuir and (b) Freundlich adsorption isotherms for Cr(VI) adsorption on the RSS-CH. (c) Langmuir and (d) Freundlich adsorption isotherms for Cr(VI) adsorption on RSS-AC.
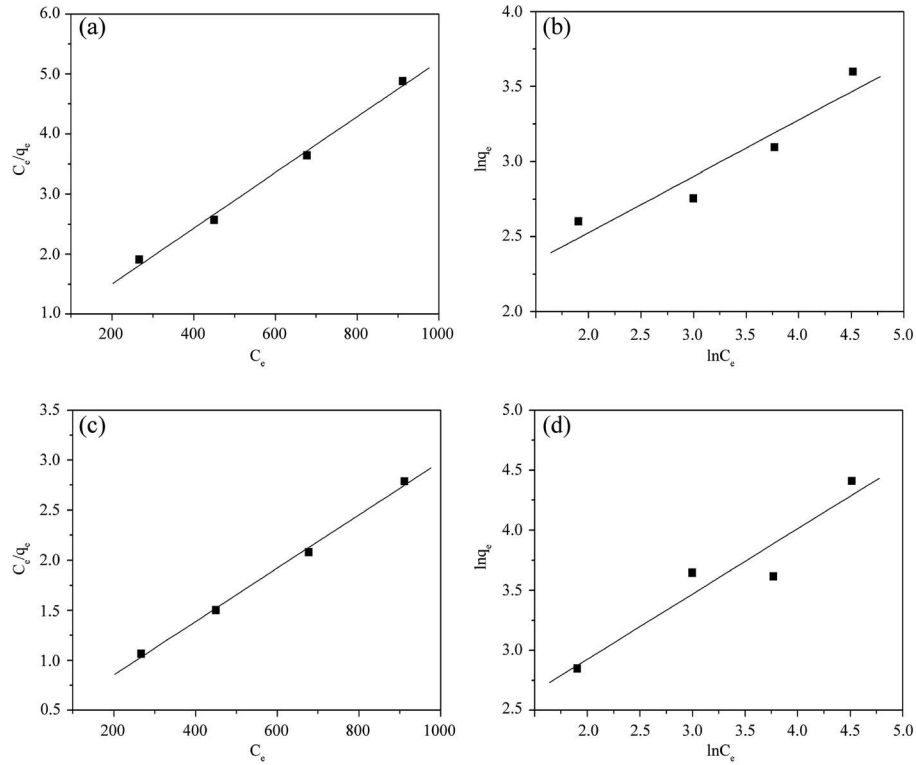
Fig. S2. (a) Langmuir and (b) Freundlich adsorption isotherms for MB adsorption on the RSS-CH. (c) Langmuir and (d) Freundlich adsorption isotherms for MB adsorption on RSS-AC.
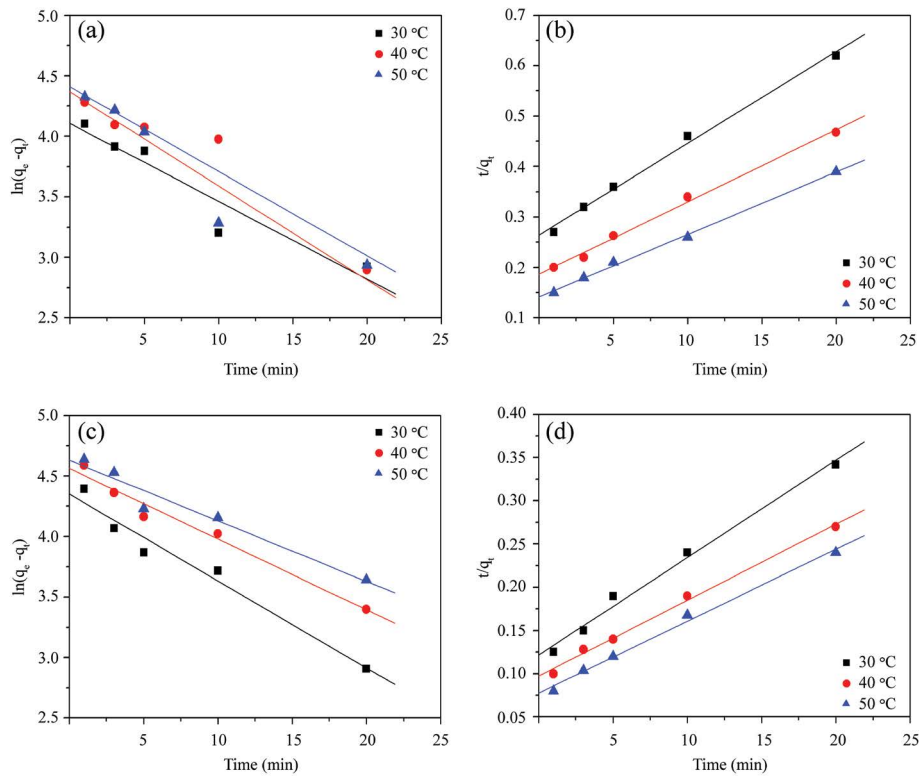

Fig. S3. Linear fit curves of (a) pseudo-first-order and (b) pseudo-second-order for Cr(VI) adsorption on the RSS-CH. Linear fit curves of (c) pseudo-first-order and (d) pseudo-second-order for Cr(VI) adsorption on RSS-AC.
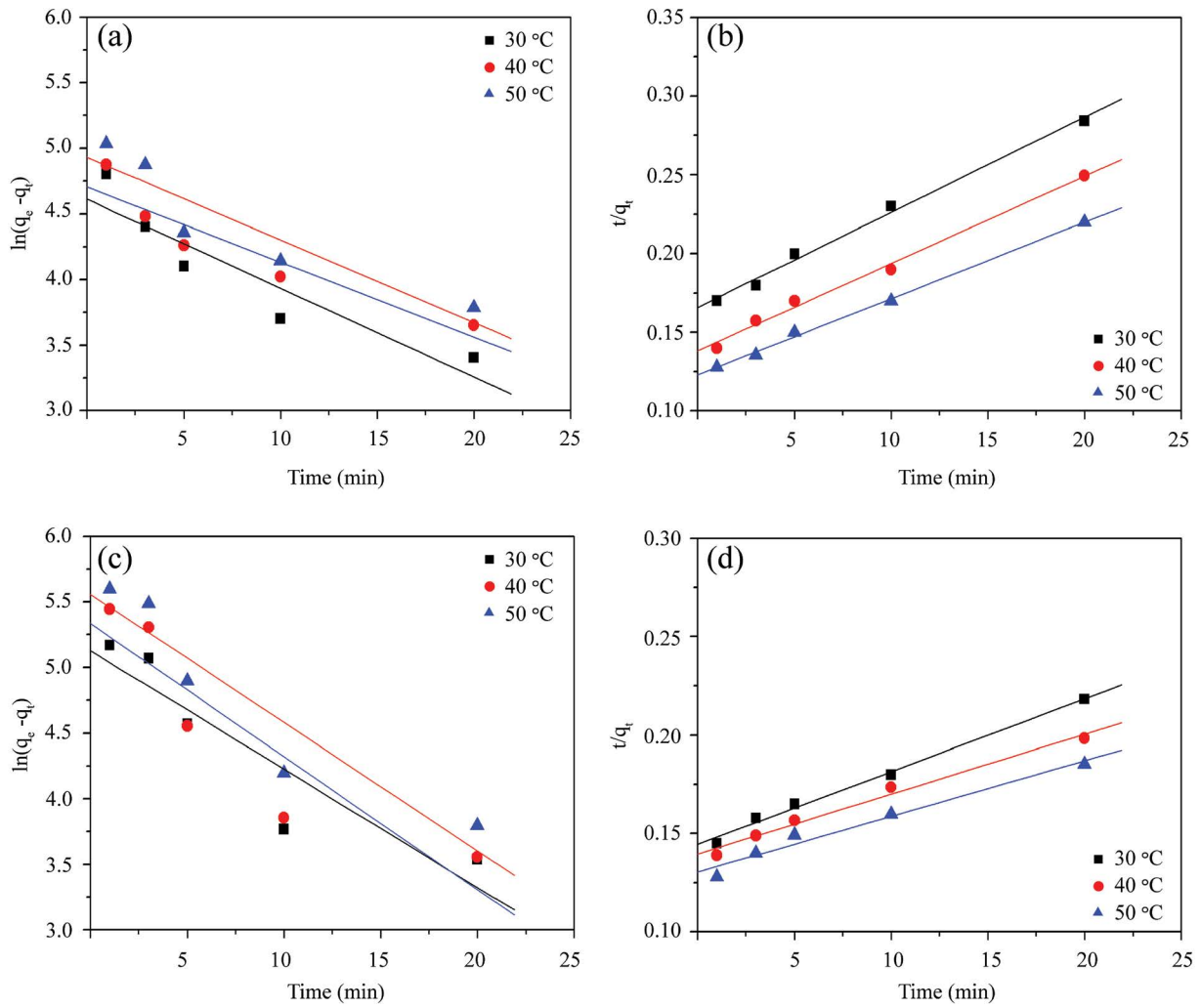
Fig. S4. Linear fit curves of (a) pseudo-first-order and (b) pseudo-second-order for MB adsorption on the RSS-CH. Linear fit curves of (c) pseudo-first-order and (d) pseudo-second-order for MB adsorption on RSS-AC.